

November
3rd, 2021

Balloni Halle,
Cologne, Germany



Stem Cell Community Day

HYBRID

COLOGNE, GERMANY – NOVEMBER 3, 2021

eppendorf

Win a prize for the best poster!

It's all about Stem Cells

Program

- > **Topics: The potential of stem cells for bioprocessing: Novel food | Cell therapy | Extracellular vesicles (Exosomes)**
- > **Pre-conference workshop "How to Culture Stem Cells in Stirred Bioreactors" on November 2, 2021 for post doctoral researchers, PhD students and lab technicians**

Confirmed speaker



- > **Professor João F. Mano**
University of Aveiro, Portugal
- > **Professor Ali Khademhosseini**
CEO and Founding Director at Terasaki Institute for Biomedical Innovation, Los Angeles, CA, USA
- > **Kevin Ullmann**
The Leibniz Research Laboratories for Biotechnology and Artificial Organs (LEBAO)

The Stem Cell Community Day 2021 will be held in a hybrid format. You have the flexibility to choose between attending the conference venue or joining the event virtually through our online events platform.

For more information: www.stemcellday.de or send us an email: stemcellday@eppendorf.de

www.eppendorf.com

Raman spectroscopy as a process analytical technology to investigate biopharmaceutical freeze concentration processes

Dennis Weber  | Jürgen Hubbuch 

Institute of Engineering in Life Sciences,
Section IV: Biomolecular Separation
Engineering, Karlsruhe Institute of Technology
(KIT), Karlsruhe, Germany

Correspondence

Jürgen Hubbuch, Institute of Engineering in
Life Sciences, Section IV: Biomolecular
Separation Engineering, Karlsruhe Institute of
Technology (KIT), Fritz-Haber-Weg 2, 76131
Karlsruhe, Germany.
Email: juergen.hubbuch@kit.edu

Abstract

Freezing processes are a well-established unit operation in the biopharmaceutical industry to increase the shelf-life of protein-based drugs. While freezing reduces degradation reaction rates, it may also exert stresses such as freeze concentration. Macroscopic freeze concentration in large-scale freezing processes has been described thoroughly by examination of frozen bulk material, but the transient process leading to such freeze concentration profiles has not been monitored yet for biopharmaceutical solutions. In this study, Raman spectroscopy as a process analytical technology is demonstrated for model formulations containing monoclonal antibodies (mAbs) or bovine serum albumin (BSA) in varying concentrations of sucrose and buffer salts. Therefore, a Raman probe was immersed into a bulk volume at different heights, monitoring the freeze concentration in the liquid phase during the freezing processes. Partial least square regression models were used to quantitatively discriminate between the protein and excipients simultaneously. The freeze concentration profiles were dependent on freezing temperature and formulation with freeze concentrations up to 2.4-fold. Convection currents at the bottom of the freezing container were observed with a maximum height of 1 mm. Furthermore, freeze concentration was correlated with the sucrose concentration in a formulation. Analysis of the freeze concentration slope indicated diffusion from the bottom to the top of the container. In summary, Raman spectroscopy is a valuable tool for process validation of freeze concentration simulations and to overcome scale-dependent challenges.

KEYWORDS

formulation, freeze concentration, monoclonal antibody, Raman spectroscopy

1 | INTRODUCTION

Pharmaceutical proteins are among the top-selling drugs with monoclonal antibodies (mAbs) as the most successful product (Shukla et al., 2017). The ever-growing demand for mAbs leads to the desire

and need for new and larger-scale manufacturing processes (Buyel et al., 2017) from which new challenges arise. As the last step, the final fill, in the production of biopharmaceutical drugs is often located off the production site, large bulk volumes of formulated drugs need transportation. To improve the shelf-life and reduce shear stress

This is an open access article under the terms of the Creative Commons Attribution-NonCommercial-NoDerivs License, which permits use and distribution in any medium, provided the original work is properly cited, the use is non-commercial and no modifications or adaptations are made.

© 2021 The Authors. *Biotechnology and Bioengineering* Published by Wiley Periodicals LLC

during transport, bulk substances may be frozen before transportation (Singh & Nema, 2010). While freezing slows down drug degradation reactions, it may also induce protein activity loss due to protein-ice surface interactions, cold denaturation, and freeze concentration gradients (Bhatnagar et al., 2007; Privalov, 1990). Therefore, drug formulations often contain excipients such as carbohydrates for protein stabilization in a glassy matrix (Connolly et al., 2015) to reduce freeze denaturation of proteins. During a freezing process, freeze concentration occurs, excluding solute molecules from the crystallizing water. On a microscale, solutes are entrapped within ice crystals and the amount of water is constantly reduced with decreasing temperatures until either a glass is formed or solutes start to crystallize. On a macroscopic scale in large-scale freezing, freezing begins at the cooling walls and progresses to the center of the container. A transition or mushy zone forms, where ice crystals grow into a solution. At this mushy freezing front, solutes are partially excluded and entrapped within the ice matrix. The solute concentration in the solid phase c_{solid} is reduced compared to the concentration c in the liquid phase at the freezing front as described by the partition coefficient k in Equation (1) (Miyawaki et al., 1998).

$$k = \frac{c_{\text{solid}}}{c}. \quad (1)$$

As a result, solute concentration and temperature gradients are found in the remaining liquid phase leading to density gradients during the freezing process. Hence, buoyancy-driven natural convection occurs in large-scale freezing processes. When observing the liquid concentration c at a fixed point, the relative freeze concentration c/c_0 , where c_0 is the initial bulk concentration, will increase over time. With increasing freezing volumes, freeze concentration profiles may change as convection becomes more dominant (Authelin et al., 2020), which poses scalability challenges. Natural convection is well described for traditional solidification processes such as alloy solidification (Shevchenko et al., 2015; Vynnycky & Kimura, 2007; Wang & Fautrelle, 2009). However, the complex solidification of multicomponent solutions frozen in pharmaceutical applications currently lacks the process understanding necessary to overcome scalability issues. In the past, studies have been performed on novel freeze-thaw devices (Geraldès et al., 2020; Roessl et al., 2014; Shamlou et al., 2007; Weber & Hubbuch, 2021) with the aim of improved scalability and processes were mostly characterized by solute concentration in the frozen bulk (Kolhe & Badkar, 2011; Miller et al., 2013; Reinsch et al., 2015; Rodrigues et al., 2012). However, in large-scale freezing processes, freeze concentration profiles are a result of the interplay of diffusive and convective mass fluxes. The analysis of the frozen bulk concentration lacks information to describe transient mass fluxes in freezing processes. First, the measured concentrations are averaged across the sample volume providing a limited spatial resolution. Second, frozen samples represent the final state with limited information on the transient freezing process. Recently, computational fluid dynamic modeling has been proposed as a tool for freeze concentration prediction (Geraldès et al., 2020; Li & Fan, 2020). While the prediction of temperature has been validated by real-time process data, the freeze

concentration profiles were only validated by the solute concentration in the frozen bulk at the end of the process. Online data of freeze concentration enables validation of simulated findings with regard to concentrations and thus improves model reliability of simulated scale-up models. The transient process of freeze concentration was investigated previously on a microscopic scale by Raman spectroscopy (Dong et al., 2009) and by Mach-Zehnder optical interferometry (Butler, 2002). Furthermore, Raman spectroscopy was also suggested as a tool for online process monitoring of pharmaceuticals (Vankeirsbilck et al., 2002). Online monitoring of the transient, macroscopic freeze concentration is yet missing. Hence, in the following study, Raman spectroscopy was used for online monitoring of macroscopic freeze concentration for the first time. Raman spectroscopy with partial-least squares (PLS) regression is used for monitoring individual formulation solutes. The transient, solute-dependent freeze concentration effects were analyzed in a large-scale freezing process. The study provides an in-depth process understanding of diffusive and convective mass fluxes present in freezing processes.

2 | MATERIALS AND METHODS

2.1 | Sample preparation

All used solutions were prepared with ultrapure water (PURELAB Ultra; ELGA LabWater; Veolia Water Technologies) and filtered using a 0.2- μm filter before application. Tris buffer was prepared from Tris-(hydroxymethyl)-aminomethane purchased from Merck and Tris-(hydroxymethyl)-aminomethane-hydrochloride purchased from AppliChem at concentrations ranging from 50 to 1500 mM. The pH was adjusted to pH 7.5 ± 0.1 using hydrochloric acid. Sucrose was used as an exemplary cryoprotectant with low tendency for crystallization (Connolly et al., 2015). Therefore, sucrose with 99% purity was purchased from former Alfa Aesar now Thermo Fisher Scientific, and dissolved at concentrations ranging from 250 to 2000 mM. All solutions were prepared from stock solutions. As a model protein, lyophilized bovine serum albumin (BSA) with a purity exceeding 98% was purchased from Merck. It was dissolved in the desired buffer solution at high concentrations using a SpeedMixer DAC 150 (Hauschild) and diluted to the desired concentration. As a typical pharmaceutical protein, a mAb was kindly provided by Byondis. The frozen cell culture supernatant was thawed and the mAb was captured using protein A chromatography. The protein A eluate was dialyzed against the buffer of interest using 10 kDa Snakeskin Dialysis Tubing from Thermo Fisher Scientific for 1 h at room temperature and then overnight at 5°C after buffer exchange. The protein concentration was adjusted using Vivaspin 2 with 30 kDa cut-off PES membranes from Sartorius and diluted with buffer.

2.2 | Experimental freezing setup

Bulk freezing was performed in an actively cooled freezing device depicted in Figure 1. The device is cooled by two individual cooling

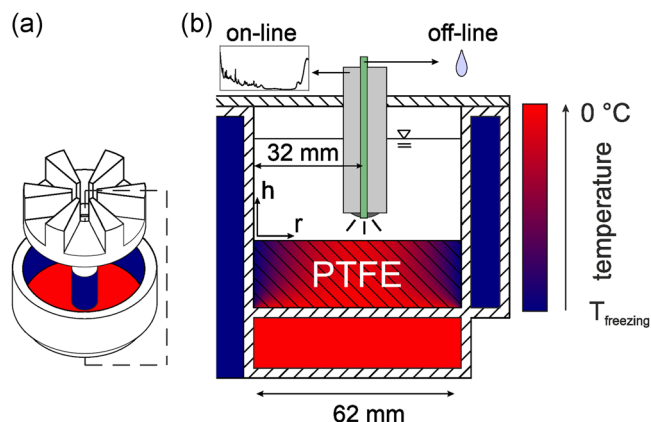


FIGURE 1 (a) An exploded view of the freeze-thaw scale-down model with the insulating inlay. The bottom temperature is controlled separately to reduce boundary effects. The freezing chamber is separated by an inlay into six chambers. A cross-section through one chamber as highlighted by the dashed box is shown in (b). The Raman probe and capillary for sampling are depicted in gray and green, respectively. Images were adapted from Weber and Hubbuch (2021). PTFE, polytetrafluoroethylene

units, one to apply the set freezing temperature and a second one to cool the bottom of the device to minimize boundary effects such as freezing from the bottom. The device is split into six individual chambers to reduce the sample volume by an inlay made from polytetrafluoroethylene (PTFE). In addition, the inlay insulates the bottom of a freezing chamber which reduces boundary effects further. An in-depth device and process characterization has been described previously (Weber & Hubbuch, 2021).

For each experiment, the freezing chamber was filled with 90 ml of process solution. If the samples were reused, the bulk was homogenized by aspirating and dispensing using a 5-ml pipette. Before a freezing process, the temperature was equilibrated for at least 2 h at 5°C, followed by the initiation of the freezing process at temperatures between -60°C and -20°C at maximum cooling rate. After the freezing step, thawing was initiated by a temperature increase to 30°C for mAb and to 40°C for BSA over at least 45 min. The individual steps were timed using predefined methods, which were executed by in-house software written with MATLAB 2020b (MathWorks). The Raman probe and the sample capillary were positioned at a distance of $r = 32$ mm from the inner cooling wall using three-dimensional (3D)-printed mounts, to assure reproducibility and precise positioning. The depth of the Raman probe was varied from 1 to 15 mm above the bottom of the freezing chamber. The exact dimensions are noted in Figure 1.

2.3 | Raman spectroscopy

A HyperFlux PRO PLUS 785 from Tornado Spectral Systems with a bandpass from 200 to 3300 cm^{-1} from 785 nm wavelength laser at a power of 495 mW together with Fiber BallProbe® from Marqmetrix

was used to obtain Raman resonance spectra. The focal length of the optics was 200 μm . The spectral resolution was 1 cm^{-1} and integration times from 700 to 1400 ms were chosen depending on the exposure time suggested by the autoexposure option of the software SpectralSoft by Tornado Spectral Systems. Spectra were recorded every 5 s. The laser probe was positioned at a constant distance from the inner cooling wall, whereas the height above the chamber bottom was varied from 1 to 15 mm as described above.

2.4 | PLS model calibration for online concentration

PLS models were calibrated from batch experiments spectra exclusively. A set of 55 solutions with varying concentrations of Tris (0–1000 mM), sucrose (0–710 mM), mAb (0–25 g/L), and BSA (0–56 g/L) were prepared from stock solutions. Calibration spectra were recorded as described above but at room temperature. For each solution, the probe height and exposure time were varied to account for possible changes in spectra background, and the spectra were recorded at least five times. The recorded spectra were processed using MATLAB R2020b (MathWorks). At least 125 of the total 775 spectra were selected for cross-validation based on equal solute concentration distribution across the measured concentrations. For preprocessing, the spectra were normalized by the exposure time, smoothed, and optionally derived using a Savitzky–Golay filter with a second-order polynomial fit (Savitzky & Golay, 1964). Wavenumbers below 700 and above 3050 cm^{-1} were excluded. A background subtraction using a water or buffer spectrum was evaluated for basic subtraction and extended multiplicative signal correction (emsc) but did not improve model accuracy and robustness. For each solute, the calibrated PLS models were used to calculate concentrations from the spectra as described by Großhans et al. (2018). Briefly, a Matlab built-in genetic algorithm was used to optimize the PLS model based on calculated predictive residual sum of squares (PRESS) with varying options such as a number of latent variables (3–10), Savitzky–Golay smoothing filter window width (5–35), and optional spectrum differentiation. Division of the PRESS by the total number of samples was used for calculation of the root mean square error cross-validation (RMSECV). Q^2 and R^2 were calculated as suggested by Wold et al. (2001). For modeling of the mAb concentration, spectra from BSA were excluded and vice versa. Furthermore, high concentrations of BSA lead to major changes in the Raman resonance. Thus, regression of the Tris concentration was performed separately for samples without and with BSA, where the latter only used information from 2700 to 3050 cm^{-1} .

2.5 | Offline sample analysis

To validate the PLS predicted concentrations, offline samples of 300 μl were taken at the same radius and height as the Raman probe using a peek capillary with an inner diameter of 0.17 mm and 1-ml

syringes. The protein concentration of the samples was measured by UV-absorption at 280 nm using a NanoDrop 2000c by Thermo Fisher Scientific. Extinction coefficients of 0.67 g/(L cm) for BSA and 1.5 g/(L cm) for mAb have been used. To determine sucrose and Tris concentrations, the conductivity and density of samples were measured using a conductivity meter CDM230 (Radiometer Analytical SAS) and microliquid density sensor (Integrated Sensing Systems, Inc). As both solutes affect both density and conductivity, a 2D regression calibration was performed with 32 samples ranging from 0 to 300 mM Tris and 0 to 1200 mM sucrose. The calibration results were approximated by second-order polynomial regression resulting in an R^2 of 0.999 for the conductivity and 0.999 for the density. Detailed calibration information is listed in the Supporting Information Material.

3 | RESULTS AND DISCUSSION

3.1 | Liquid freeze concentration monitoring with Raman spectroscopy

The freezing process of pharmaceutical formulations was evaluated using Raman resonance spectroscopy. Spectral changes over the course of a freezing process may occur due to for example temperature deviation presented and discussed in the following. The Raman spectrum of a purified water sample measured in the freezing chamber at room temperature contained peaks at 1637 and 3235 cm^{-1} attributed to water and peaks at 732, 1215, 1300, and 1380 that occur due to the PTFE (Schmälzlin et al., 2014) bottom of the freezing chamber. The transition from water to ice can be observed in the spectra at 3140 cm^{-1} , where a distinct ice peak arises, while the water peak at 3235 cm^{-1} declines as the solution freezes as shown in Figure 2b. The ice peak was described and compared already in the early 1930s by Ockman (1958) and the

transition during solidification was recently used to describe phase transition from water to ice (Đuričković et al., 2011). In addition, baseline shifts were present throughout all measurements, which are comparable to Raman spectra of biological samples (Guo et al., 2016) in the fingerprint region from 700 to 1900 cm^{-1} and due to the broad water resonance peak from 2600 to 3330 cm^{-1} . The addition of solutes leads to numerous peaks in the fingerprint region and from 2600 to 3050 cm^{-1} , as well as baseline shift changes in the fingerprint region. The spectra observed at 5 mm above the bottom for a model formulation with 50 mM Tris and 200 mM sucrose frozen at -20°C is depicted in Figure 2.

As shown in Figure 2a, the spectra remain stable until around 30 min when freezing at -20°C . After 30 min, most of the peaks in the fingerprint region began to increase due to freeze concentration. Water peaks, however, remained constant until solidification began. When the freezing front reached the Raman probe, ice crystals are formed leading to a significant decrease of the mean Raman resonance as shown in Figure 2c. The decrease of the mean spectrum can be attributed to changes in optical density due to crystallization. Thus, the rapid decrease in the mean spectra was used to detect the beginning of the phase change. Đuričković et al. (2011) suggested using a ratio S_D of water and ice peak areas to describe the phase transition. Similarly, S_D was calculated after Equation (2) by summing up the raw Raman intensities I for the water peak area from 3270 to 3290 cm^{-1} and the ice area from 3140 to 3160 cm^{-1} . When comparing the mean Raman resonance and S_D , as shown in Figure 2c, both signals decreased upon arrival of the freezing front at the Raman probe after 44 min. The mean Raman signal decreased rapidly and stabilized after 60 min total, whereas S_D decreased later and continuously decreases over the observed time. This indicates, that the majority of solidification has taken place after 16 min and optical properties reached an equilibrium. Meanwhile, the water crystals are continuously formed and the ice structure changes as seen in S_D , while the solution is approaching phase equilibrium given for the

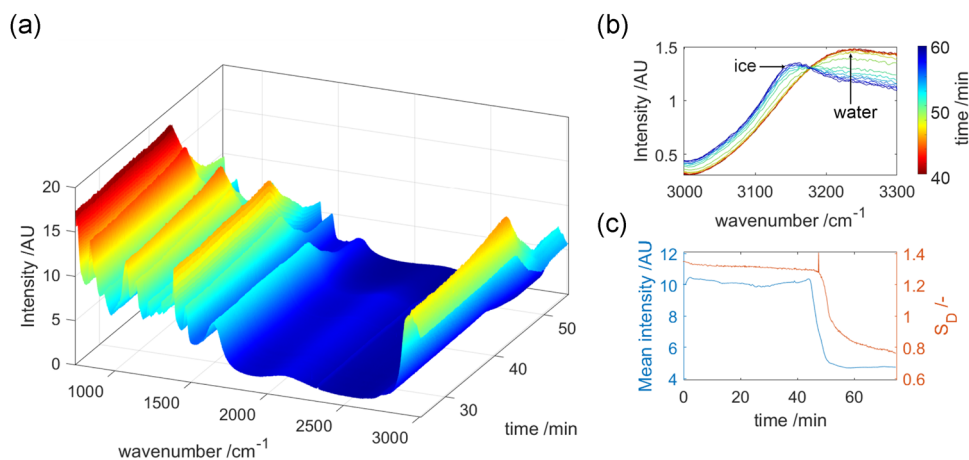


FIGURE 2 (a) Example Raman spectra over time when freezing a 50 mM Tris, 200 mM sucrose solution at -20°C . Probe height was 5 mm. (b) Raman spectra shift from water to ice used for calculation of S_D . (c) Comparison of the mean spectrum and the water to ice peak areas S_D over time.

current temperature. Ideally, the method would be able to predict the solute concentration in the frozen state. However, PLS modeling of freeze concentrated solution would require frozen solutes with known concentration for model calibration. Due to microscale freeze concentration within the crystalline ice structure, this was not possible with the used set-up. Twomey et al. overcame this issue by the implementation of confocal Raman spectroscopy (Twomey et al., 2015). In this study, the application of PLS models derived from liquid samples on frozen state, however, resulted in large differences for Tris and sucrose as shown below in Section 3.3, and predicted concentrations postfreezing were not reproducible. The Raman probe and laser introduce heat in the system, influencing the ice structure and glass composition. Thus, the predictions of concentration are only valid in the liquid state and the freeze concentration data postfreezing is not shown in the following for visualization purposes.

$$S_D = \frac{\sum_{3270}^{3290} I}{\sum_{3140}^{3160} I} \quad (2)$$

3.2 | PLS modeling of Raman spectra for concentration quantification

PLS models were used to quantify and distinguish up to three individual formulation agents. PLS regression coefficient of each solute is shown in Figure 3 and the PLS modeling characteristics are summarized in Table 1.

For all solutes except BSA, the first derivative of the spectra led to the best modeling results. While one PLS model for sucrose quantification could be used for all samples, a separate model for Tris quantification was used for samples containing BSA, where only the wavenumbers from 2700 to 3050 cm^{-1} were used. In general, three to nine latent variables have been used with a Savitzky-Golay filter window between 5 and 19 wavenumbers. Other studies used five to seven latent variables (Filik & Stone, 2007; Parachalil et al., 2018) for the prediction of protein concentrations with Raman spectroscopy. The calculated coefficients of determination R^2 ranged from 0.997 to 0.999 with similar Q^2 values. The models provided a good linear correlation across all the calibration concentrations. Despite the promising quality attributes of the models, the model data was generated solely from batch measurements at room temperature. Temperature changes and convection in the freezing process might cause background variations and noise reducing model accuracy. Therefore, validation of the predictions in freezing processes was performed to evaluate deviations from batch measurements as discussed later. Spectral preprocessing to minimize the influence of process conditions on the model was evaluated by emsc and subtraction of a water spectrum as a background. However, this intense preprocessing did not improve the model by means of R^2 and predicted high noise levels when applied to freeze process data. Furthermore, spectrum normalization, while giving the opportunity of overcoming challenges in optical property shift, also led to worse R^2

values and high signal-to-noise ratios in the predicted concentrations in the process.

3.3 | Validation of Raman concentration monitoring

To validate PLS predicted freeze concentration, the predicted concentrations were compared against concentrations in liquid samples, that were aspirated at a 5 min interval using a capillary. The Raman probe and capillary were positioned 5 mm above the chamber bottom at an equal distance from the inner freezing wall, as indicated in Figure 1b. Two studies with and without protein were performed. First, a 200 mM sucrose, 100 mM Tris solution at pH 7.5 was frozen at -20°C , and concentrations measured and predicted are shown in Figure 4.

Between 5 and 30 min, the solute concentration remained stable with offline concentrations of 106 ± 1.2 mM Tris and 197 ± 2.5 mM sucrose and online predicted concentrations of 112 ± 3.6 mM Tris and 203 ± 3.0 mM sucrose. The agreeing measurements and the low signal variation highlight the PLS model accuracy and the robustness with regard to noise. After 30 min, the solute concentration of Tris and sucrose increased in both online and offline measurements. While offline measurements showed maximum concentrations of 189 mM Tris and 338 mM sucrose after 50 min, the Raman spectra indicated concentrations of 171 mM Tris and 315 mM sucrose. The differences may be attributed to continuous extraction of concentrated samples at the capillary thus adding a source of turbulence and mixing. As a result of the mixing, the higher concentrated solution might be aspirated from the lower layers, as shown later. After

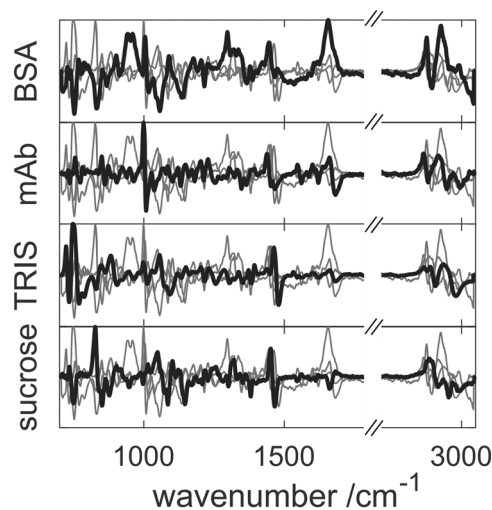


FIGURE 3 Normalized partial least square regression coefficients for the prediction of solute concentration. The regression coefficients of the solute are highlighted as a bold line, while the remaining coefficients are supplemented in gray. Bovine serum albumin (BSA) spectra are nonderived. Monoclonal antibody (mAb), Tris, and sucrose coefficients are applied to the first derivative of a spectrum

	mAb	sucrose	Tris	BSA	Tris (with BSA)
Latent variables	8	7	5	9	3
Savitzky-Golay window	11	29	19	15	5
Derivative	1	1	1	0	1
Wavenumbers /cm ⁻¹	700–3050	700–3050	700–3050	700–3050	2700–3050
R ²	0.998	0.997	0.999	0.999	0.939
Q ²	0.999	0.999	1.000	1.000	0.999
RMSECV	0.07 g/L	1.08 mM	0.72 mM	0.08 g/L	2.56 mM
Calibration range	1.7–25 g/L	80–708 mM	31–1000 mM	14–56 g/L	31–1000 mM

Note: Two Tris models were used for prediction in the presence and without BSA.

Abbreviations: BSA, bovine serum albumin; mAb, monoclonal antibody; PLS, partial least square; Q², cross-validated R²; R², coefficient of determination; RMSECV, root mean square error cross-validation.

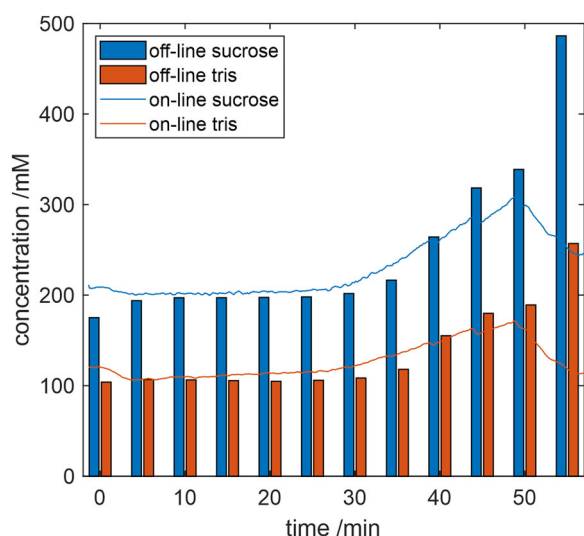


FIGURE 4 Freeze concentration predictions online with Raman and offline by sampling at a 5-min interval. The Raman probe was positioned 5 mm above ground. Tris and sucrose determination by conductivity and density

50 min, the freezing front reached both the Raman probe and the capillary leading to an apparent decrease in online predicted concentration. The offline measurements, on the other hand, indicated a steep increase in concentration. While the arrival of the freezing front was clearly detected by Raman spectroscopy, liquid sampling was still possible. The offline measurements did no longer measure the bulk concentration but instead, the freeze concentrated liquid extracted through the capillary. Furthermore, the end of the capillary was located approximately 7 mm away from the Raman probe focal point. Due to the thermal impact of the Raman probe, freeze concentration might have been impacted by the probe itself.

TABLE 1 Summary of the Raman spectrum preprocessing parameters, the PLS model parameters, and the quality of prediction for each solute

When examining the freeze concentration of a highly concentrated BSA solution with 56 g/L BSA, 100 mM Tris, and 225 mM sucrose at pH 7.5, similar results were found, as shown in Figure 5. From 0 to 30 min, 59.3 ± 1.1 g/L BSA, 99.4 ± 8.6 mM Tris, and 222.9 ± 2.3 mM sucrose were predicted and 56 ± 0.4 g/L BSA were measured offline. In general, the predicted concentrations show an offset to the initial concentration of 3 g/L. Adding BSA to the formulation significantly decreased the PLS model robustness of Tris, as standard deviations of up to 9% were observed over the first 25 min compared to 3% without BSA. Looking at the relative freeze concentration (c/c_0) shown in Figure 5b, the BSA concentration increased by 38% detected by Raman and by 37% measured offline after 57 min (offline increase interpolated linearly). The root mean square error of prediction (RMSEP) between measured and predicted BSA concentrations was 3.8 g/L absolute and 1.5% for relative concentrations. In comparison, Parachalil et al. (2018) reported an RMSECV of 1.58 g/L for albumin quantification by Raman spectroscopy from 5 to 50 g/L and Filik and Stone (2007) reported RMSEPs of 8%–11% of the mean concentration, which is in range with our model. Other models report lower RMSEPs around 1 mM for glucose (Rohleder et al., 2005), but have a smaller upper calibration limit of 24 mM. The presented model focuses on the determination of the relative freeze concentration rather than the exact quantification of solutes.

3.4 | Freeze concentration at different temperatures

A highly concentrated BSA solution of 50 g/L BSA, 50 mM Tris, 225 mM sucrose at pH 7.5 was frozen at different temperatures and monitored with the Raman probe 5 mm above the ground. The influence of the freezing temperature on the freeze concentration

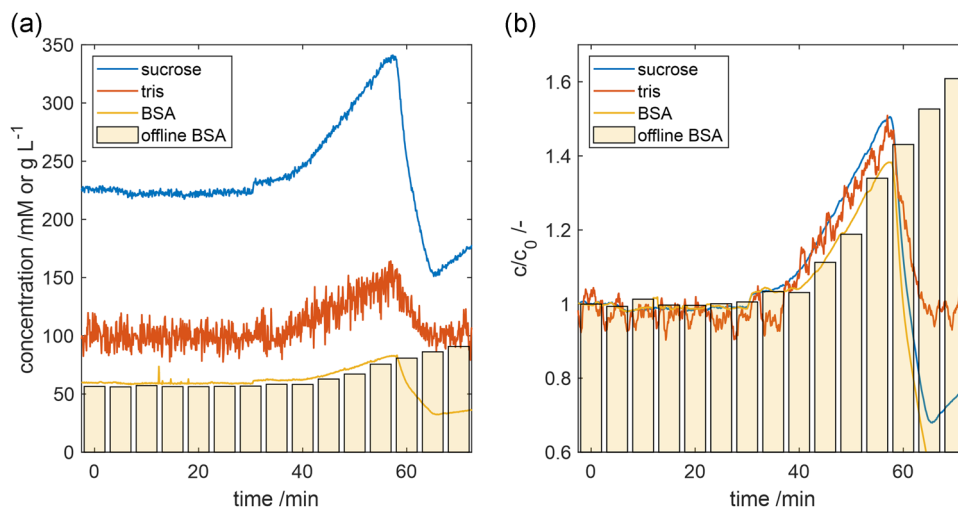


FIGURE 5 Freeze concentration predicted online with Raman and measured offline by sampling at a 5 min interval. The Raman probe was positioned 5 mm above ground. Bovine serum albumin (BSA) concentration determined by UV-Vis absorption at 280 nm. (a) Absolute concentrations. (b) Concentrations normalized by initial values

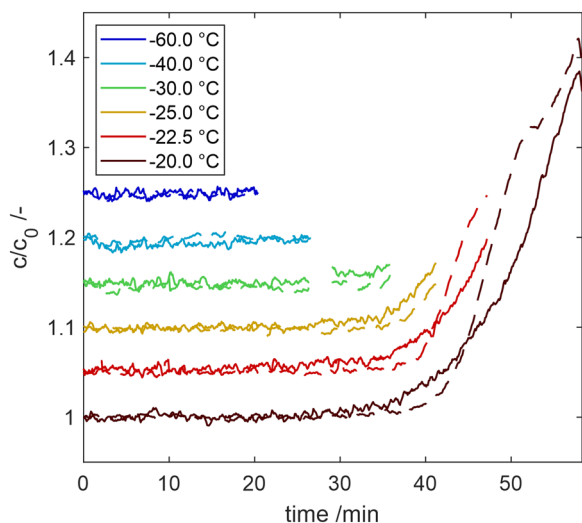


FIGURE 6 Sucrose (-) and Bovine serum albumin (BSA) (--) relative freeze concentration at different freezing temperatures. The Raman probe was positioned 5 mm above ground. Concentrations are shifted by 0.05 for visualization purposes. Outliers at -30°C were excluded

profile was investigated. Within the first 5 min of all freezing experiments shown in Figures 6 and 7, concentrations of 51 ± 0.6 g/L BSA, 32 ± 2.2 mM Tris, and 235 ± 3.2 mM sucrose were predicted. As starting concentrations c_0 remain the same across the experiments, only relative concentrations (c/c_0) of BSA and sucrose are described and discussed in the following.

As expected, the freezing time was reduced with decreasing freezing temperatures. In addition, freeze concentration was not observed when freezing at -40°C or below. For higher freezing temperatures, the freeze concentration at the time of freezing

increases with temperature. The correlation of freezing time t to the negative inverse of cooling temperature T_{cooling} ($t \sim -1/T_{\text{cooling}}$) as well as similar freeze concentration behavior in frozen bulk media was shown previously (Weber & Hubbuch, 2021).

Looking at the freeze concentration of BSA, the concentration began to increase later than the sucrose concentration after 35–40 min and quickly exceeded the sucrose concentration. The maximum relative concentration difference between BSA and sucrose ($c_{\text{BSA}}/c_{\text{BSA},0} - c_{\text{sucrose}}/c_{\text{sucrose},0}$) occurring at -20°C was 11.8% after 51 min and narrowed down over time to 3.1% after 58 min.

Interestingly, the freeze concentration showed a similar progression over time throughout all examined freezing temperatures. For example, the relative sucrose concentration exceeds the BSA freeze concentration for all experiments between 20 and 30 min. More specifically, the relative sucrose concentration increased by $1.4 \pm 0.25\%$ after 35 min across freezing temperatures from -20°C to -30°C and after 40 min by $4.6 \pm 0.87\%$ across freezing temperatures from -20°C to -25°C . This indicates, that freeze concentration and thus the partition coefficient in larger pharmaceutical tanks might be primarily dependent on freezing time. Natural convection can explain this phenomenon as illustrated in Figure 8.

The freezing time correlates with the freeze front velocity, which increased with lower freezing temperatures in this study. However, the freeze concentration was similar over time at different freezing temperatures and thus independent from the freeze front velocity. If the natural convection was negligible, the concentration profile at the freezing front would be dominated by diffusion forming a diffusive concentration layer. This diffusive layer would lead to a similar freeze concentration at the end of each freezing process across varying temperatures when the layer reaches the Raman probe. In this study, however, the opposite was found. Convection dominated the freezing processes dragging the concentrated solutes from the freezing

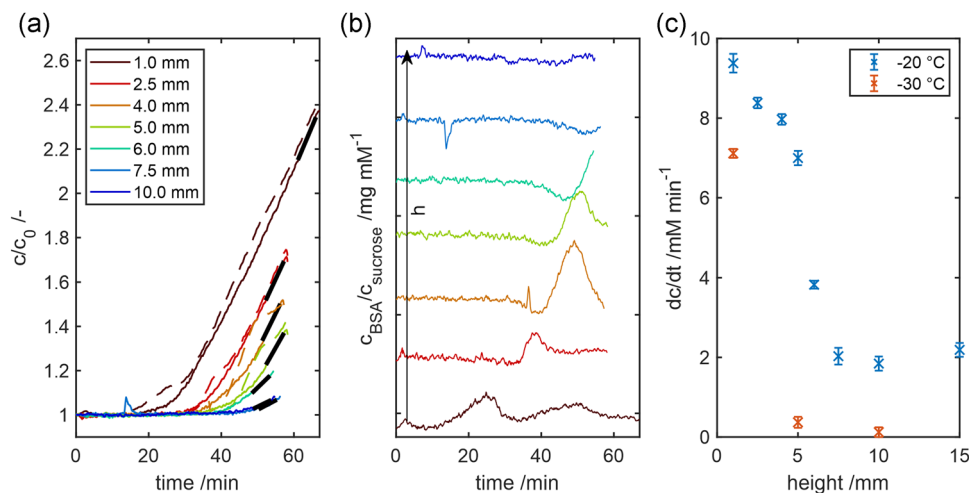


FIGURE 7 Freeze concentration of bovine serum albumin (BSA) formulation at different heights. (a) freeze concentration at -20°C of BSA (--) and sucrose (-). (b) freeze concentration at -20°C of BSA relative to sucrose over time for different heights h . The color scheme in (a) and (b) is the same. Lines are shifted by increments of 0.03 for visualization purposes. (c) final freeze concentration slope of sucrose before freezing as indicated by solid black lines in (a)

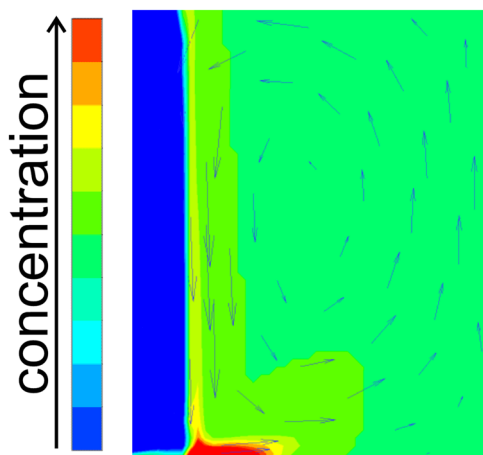


FIGURE 8 Schematic of a freeze concentration profile. The freezing front moves from the left, cooling wall towards the center. Liquid currents are displayed by arrows, where the velocity is represented by arrow length. Diffusion occurs orthogonal to isoconcentration lines. Convective mass transport drags solute enriched liquid along the bottom of the chamber from where it diffuses to the top

front along the bottom to the center and thus reducing the formation of a diffusive layer. Low convection current flow rates are expected at the freezing front and the container bottom. Hence, the current at the bottom needs time to reach the Raman probe. For shorter freezing times at low freezing temperatures faster freeze front velocities will occur. The convective current at the bottom might be slower and thus freeze concentrated solution is entrapped. Hence, similar freeze concentration profiles independent from the freezing temperature indicate convective flow. In addition, similar freeze concentration profiles indicate a constant partition coefficient independent of the freezing temperature. Butler (2002) evaluated the

freeze concentration in smaller thin films without convection and found a constant partition coefficient. It was used to describe freeze concentration by a quasi-steady-state approximation valid for low molecular weight solutes and at slow freezing speeds.

3.5 | Freeze concentration at different heights

As indicated in Figure 8, natural convection drags freeze concentrated solution to the bottom of a container, and freeze concentration-time profiles will change along a vertical axis. Therefore, the model solution, containing 50 g/L BSA, 50 mM Tris, and 225 mM Sucrose at pH 7.5, was frozen at -20°C and monitored at different heights from 1 to 15 mm above the ground. The relative freeze concentration behavior of BSA and sucrose at the different levels is depicted in Figure 7a.

The relative freeze concentration was detected first at the bottom of the container and continuously progressed throughout the different layers. More specifically, the sucrose freeze concentration exceeded 101% after 19, 30, 33, 35, 37, and after 45 min at heights of 1, 2.5, 4, 5, 6, and 7.5 mm, respectively. The freeze concentration of BSA was detected before sucrose at the bottom of the container but was delayed at elevated heights. The relative freeze concentration of BSA exceeded 101% after 13, 31, 35, 38, 43, and 52 min at heights of 1, 2.5, 4, 5, 6, and 7.5 mm, respectively.

As freezing continued, the freeze concentration of sucrose increased exponentially at the beginning and turned into a linear, steady concentration increase. The maximum relative freeze concentration 1 mm above ground was 2.42-fold for BSA and 2.38-fold for sucrose. It decreased rapidly over height to a 1.42-fold BSA and 1.38-fold sucrose freeze concentration at 5 mm. Other studies evaluated the freeze concentration in a frozen cylindrical vessel by slicing the frozen bulk in 7 mm thick layers and found a twofold to threefold

increase of BSA and trehalose (Rodrigues et al., 2011). Roessler et al. (2014) found freeze concentrations of up to 2.5-fold for lactic dehydrogenase and phosphate for frozen sampling over 14 mm sample height. While the results from this study are within the range of the previously described freeze concentrations, they indicate that the freeze concentration measured by frozen sampling may underestimate the maximum freeze concentration by up to onefold as it evaluates the average freeze concentration over a sample height.

The ratio of BSA to sucrose concentration is shown in Figure 7b. When comparing the freeze concentration of BSA to the freeze concentration of sucrose, it appears, that an initial peak of BSA was transported from the bottom to the top of the freezing chamber. Right before freezing, the ratio of BSA to sucrose concentration ($(c_{\text{BSA, end}}/c_{\text{BSA, 0}})/(c_{\text{sucrose, end}}/c_{\text{sucrose, 0}})$) was similar across all heights with 1.01 ± 0.02 -fold. As these results are the first description of online monitored freeze concentration, the following hypothesis is derived. The maximum natural convection occurs at the beginning of freezing processes (Gerald et al., 2020), as the highest density gradients are formed due to the initial large temperature differences in the bulk medium. Higher concentrations of BSA compared to sucrose might be dragged to the bottom of the container. Two potential reasons are a smaller partition coefficient leading to higher exclusion from the freezing front and/or slower diffusion of the larger molecule (Torres et al., 2012). The current velocity at the freezing front declines over the distance from the freezing front as shown in Figure 8. With increasing diffusion coefficients, molecules diffuse further into the convective current due to the orthogonality of the concentration gradient and the convection current. Thus, the freeze concentration at the bottom is a complex interplay between diffusive and convective mass transport at the freezing front. With comparably slow diffusion, BSA might initially not be able to escape the convection flux in contrast to the smaller sucrose molecules. Over time, BSA is dragged to the container bottom by convection. From there it diffuses vertically to the top of the container as the concentration at the bottom continuously increases by convection. This may lead to an initial BSA-rich concentration peak first detected at the bottom.

Under the assumption of the negligible contribution of convective mass transport along the observed vertical axis, the data can be used to evaluate the impact of the diffusive flux according to Fick's second law, which describes diffusion over time driven by spatial concentration differences (Fick, 1855). However, due to the necessity of second-order derivation in space, a low number of selected spatial measurements are not sufficient to provide a reliable dataset. An external long-distance focal point Raman probe could be used for spatially resolved datasets to overcome this issue. In this study, however, mass fluxes can only be interpreted on a qualitative scale. Thus, the slopes of the sucrose freeze concentration over time right before freezing have been fitted, as indicated in Figure 7a, and are shown in Figure 7c for temperatures of -20°C and -30°C . From the bottom of the freezing chamber, where the concentration is continuously increased by convection, the concentration slope declines until approximately 7.5 mm above ground, where stagnant slopes were present. The continuously decreasing slopes over the height indicate the degree of diffusion and support the hypothesis of diffusion

from the bottom to the top of the container. In addition, the decreasing slopes over height, as well as steadily increasing concentrations, imply low turbulences in the freezing process and thus laminar flow. On the other hand, the stagnant slopes in higher layers indicate a diffusion layer in front of the mushy freezing zone that has formed over time. The diffusive layer at the freezing front reaches the Raman probe at a similar time across the entire height, explaining the similar degree of freeze concentration found at elevated heights. Exemplarily measured freeze concentration at -30°C at three heights showed reduced freeze concentration slope without hardly any detected diffusion layer as shown by the slopes in Figure 7c.

Finally, with increasing distance between probe and chamber ground, the freezing time increased. This can be attributed to the impact of the stainless-steel probe due to heat conduction of the room temperature through the insulation into the freezing chamber. For further studies, this might be avoided by the use of an external Raman probe with a long focal distance.

3.6 | Formulation dependent freeze concentration

Lastly, the influence of solute concentration on the freeze concentration behavior was investigated for common industrial formulation components. An industrial formulation was mimicked by a mAb formulated in Tris and varying concentrations of stabilizing sucrose. The solutions were frozen at -20°C and the freeze concentration was monitored at a height of 5 mm. The freeze concentration profiles are depicted in Figure 9.

The formulations contained 4 g/L mAb, 50 mM Tris, and 100–300 mM sucrose at pH 7.5. The initially predicted concentrations were 3.9 ± 0.14 g/L mAb, 49.6 ± 2.3 mM Tris, and 105, 159, 211, 289 mM sucrose for the individual formulations. This indicates the model accuracy and in the following, only the relative freeze concentration (c/c_0) will be described. In general, the maximum freeze concentration of mAb increased with sucrose concentration. Maximum freeze concentrations of 1.28-fold mAb, 1.33-fold Tris, and 1.37-fold sucrose were observed right before freezing. Similar to the BSA case study, low molecular solutes were concentrated to a similar degree. The mAb, however, was the least freeze concentrated for all formulations. As mAb with approximately 150 kDa is larger than BSA with 66 kDa, it has a lower diffusion coefficient (Torres et al., 2012). Diffusion towards the center reduces the concentration at the freezing front. As shown in Equation (1), the amount of solute encapsulated at the freezing front is dependent on the solute concentration at the freezing front. Thus, larger proteins may experience overall less freeze concentration as they are entrapped by the freezing front to a higher degree, which agrees with the freeze concentration of different proteins in the cell culture supernatant (Weber et al., 2021). Kolhe and Badkar (2011) also reported significant differences in sugar and mAb freeze concentration for solutions frozen in bottles. However, the diffusion of the proteins in the two cases is also dependent on the viscosity, which is different for the BSA and mAb formulation.

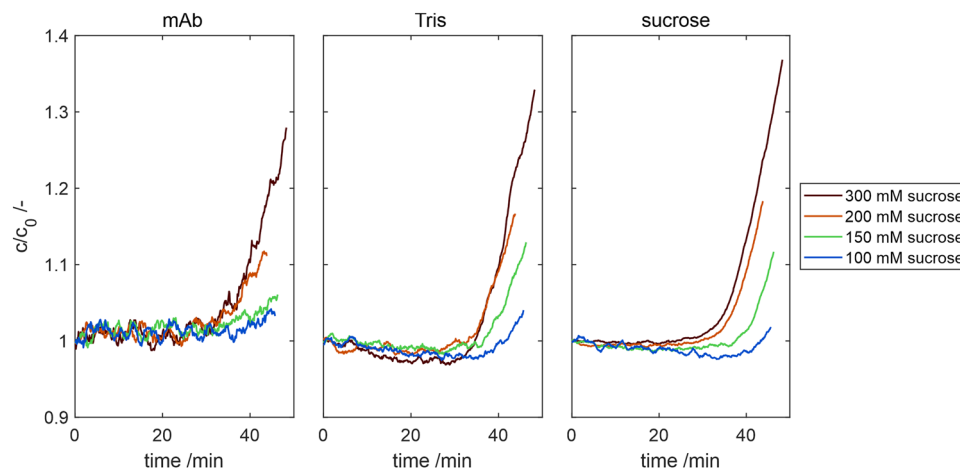


FIGURE 9 Freeze concentration predictions for monoclonal antibody (mAb), Tris, and sucrose in formulations with varying amounts of sucrose from 100 to 300 mM. The Raman probe was positioned 5 mm above ground.

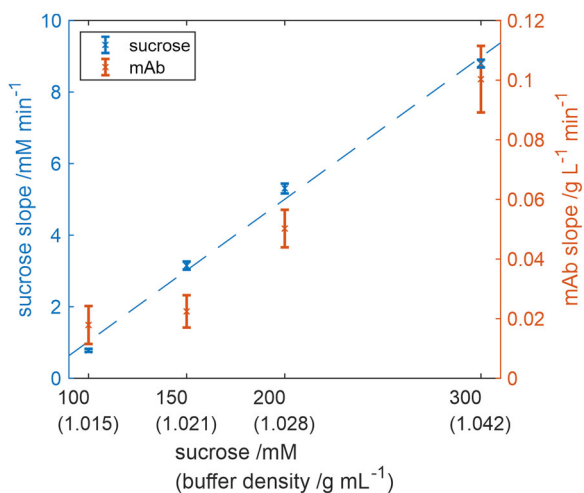


FIGURE 10 Final freeze concentration slope of sucrose and monoclonal antibody (mAb) before freezing as a function of sucrose concentration. The dashed line represents a linear regression of the sucrose slopes. The density of the formulating buffers is proportional to the sucrose concentration and denoted in parentheses

In addition to that, the final slope of freeze concentration before freezing increased with sucrose concentration for both mAb and sucrose as shown in Figure 10. The outlier of mAb freeze concentration at 100 mM sucrose can be attributed to the comparably high noise of the prediction.

Next to higher overall freeze concentration, high sucrose concentrations also led to earlier detection of freeze concentration. Under the assumption of a similar partition coefficient for the given concentrations, more molecules are excluded from the ice matrix upon freezing with increasing concentrations resulting in higher absolute concentration gradients in the liquid phase. Because the measured buffer density is proportional to the sucrose concentration, higher density gradients in the bulk solution will occur leading to increased convection. In contrast to the BSA freeze concentration,

freeze concentration of mAb and sucrose occurred at approximately the same time despite different diffusion coefficients, suggesting that the initial freeze concentration is dominated by convection for formulations with low concentrations of mAb. Furthermore, the viscosity also increases with the sucrose concentration, which reduces diffusive and convective mass transport. For further investigation of convective mass transport in freezing processes, the Grashof number should be evaluated at increasing additive concentrations, requiring the determination of freeze concentration at the freezing front. A coupling of diffusive models and computational fluid dynamics might add to the process understanding of mass transport effects.

4 | CONCLUSION

In this study, Raman resonance spectroscopy was thoroughly investigated as a novel approach for process monitoring of pharmaceutical freezing processes. While the previous characterization of freeze concentration was limited on the frozen bulk, Raman spectroscopy gives a deeper process understanding of the origin freeze concentration profiles in frozen bulk volumes. Current low-resolution frozen sampling might underestimate freeze concentration by many-fold, as convective flows were in dimensions of 1 mm or thinner. This highlights the importance of spatial high-resolved data acquired by Raman spectroscopy. The qualitative evaluations of diffusional and convective mass fluxes are a powerful tool for the optimization of freezing processes with regard to process parameters such as temperature and formulation composition. Further information could be retrieved by using an external Raman probe with a long-distance focal length scanning for freeze concentration. This study contributes to quality-by-design freezing processes and formulation development. Product loss due to transient freeze concentration effects can be identified and reduced. The method provides the first real-time data of freezing processes for the validation of scale-down models as well as simulations. Process characterization by Raman monitoring provides proven acceptable and normal ranges for regulatory authorities.

ACKNOWLEDGMENTS

The authors would like to express their gratitude for the financial support by Bilfinger Industrietechnik Salzburg GmbH, Schwetzingen, Germany, for the material supply by Byondis Nijmegen, the Netherlands and for provision of the Raman spectrometer by Sanofi-Aventis Deutschland GmbH, Frankfurt, Germany. Furthermore, the authors would like to thank Nils Hillebrandt, Michel Eppink, and Bas Kokke for proofreading the manuscript and Jan Kehrbaum for his assistance in the laboratory. The authors declare no conflict of interest. Open Access funding enabled and organized by Projekt DEAL.

CONFLICT OF INTERESTS

The authors declare that there are no conflict of interests.

DATA AVAILABILITY STATEMENT

The data that support the findings of this study are available from the corresponding author upon reasonable request.

ORCID

Dennis Weber  <https://orcid.org/0000-0002-8700-579X>

Jürgen Hubbuch  <https://orcid.org/0000-0003-0839-561X>

REFERENCES

- Authelin, J. R., Rodrigues, M. A., Tchessalov, S., Singh, S. K., McCoy, T., Wang, S., & Shalaev, E. (2020). Freezing of biologicals revisited: Scale, stability, excipients, and degradation stresses. *Journal of Pharmaceutical Sciences*, 109, 44–61. <https://doi.org/10.1016/j.xphs.2019.10.062>
- Bhatnagar, B. S., Bogner, R. H., & Pikal, M. J. (2007). Protein stability during freezing: Separation of stresses and mechanisms of protein stabilization. *Pharmaceutical Development and Technology*, 12(5), 505–523. <https://doi.org/10.1080/10837450701481157>
- Butler, M. F. (2002). Freeze concentration of solutes at the ice/solution interface studied by optical interferometry. *Crystal Growth and Design*, 2(6), 541–548. <https://doi.org/10.1021/cg025591e>
- Buyel, J. F., Twyman, R. M., & Fischer, R. (2017). Very-large-scale production of antibodies in plants: The biologization of manufacturing. *Biotechnology Advances*, 35(4), 458–465. <https://doi.org/10.1016/j.biotechadv.2017.03.011>
- Connolly, B. D., Le, L., Patapoff, T. W., Cromwell, M. E. M., Moore, J. M. R., & Lam, P. (2015). Protein aggregation in frozen trehalose formulations: Effects of composition, cooling rate, and storage temperature. *Journal of Pharmaceutical Sciences*, 104(12), 4170–4184. <https://doi.org/10.1002/jps.24646>
- Dong, J., Hubel, A., Bischof, J. C., & Aksan, A. (2009). Freezing-induced phase separation and spatial microheterogeneity in protein solutions. *Journal of Physical Chemistry B*, 113(30), 10081–10087. <https://doi.org/10.1021/jp809710d>
- Đuričković, I., Clavier, R., Bourson, P., Marchetti, M., Chassot, J. M., & Fontana, M. D. (2011). Water-ice phase transition probed by Raman spectroscopy. *Journal of Raman Spectroscopy*, 42(6), 1408–1412. <https://doi.org/10.1002/jrs.2841>
- Fick, A. (1855). Über Diffusion [Translated: (1995) "On liquid diffusion". *Journal of Membrane Science*]. *Poggendorff's Annalen Der Physik Und Chemie*, 94(1), 59–86.
- Filik, J., & Stone, N. (2007). Drop coating deposition Raman spectroscopy of protein mixtures. *Analyst*, 132(6), 544–550. <https://doi.org/10.1039/b701541k>
- Geraldes, V., Gomes, D. C., Rego, P., Fegley, D., & Rodrigues, M. A. (2020). A new perspective on scale-down strategies for freezing of biopharmaceuticals by means of computational fluid dynamics. *Journal of Pharmaceutical Sciences*, 109(6), 1978–1989. <https://doi.org/10.1016/j.xphs.2020.02.012>
- Großhans, S., Rüdte, M., Sanden, A., Brestrich, N., Morgenstern, J., Heissler, S., & Hubbuch, J. (2018). In-line Fourier-transform infrared spectroscopy as a versatile process analytical technology for preparative protein chromatography. *Journal of Chromatography A*, 1547, 37–44. <https://doi.org/10.1016/j.chroma.2018.03.005>
- Guo, S., Bocklitz, T., & Popp, J. (2016). Optimization of Raman-spectrum baseline correction in biological application. *Analyst*, 141(8), 2396–2404. <https://doi.org/10.1039/c6an00041j>
- Kolhe, P., & Badkar, A. (2011). Protein and solute distribution in drug substance containers during frozen storage and post-thawing: A tool to understand and define freezing-thawing parameters in biotechnology process development. *Biotechnology Progress*, 27(2), 494–504. <https://doi.org/10.1002/btpr.530>
- Li, J. Q., & Fan, T. H. (2020). Phase-field modeling of macroscopic freezing dynamics in a cylindrical vessel. *International Journal of Heat and Mass Transfer*, 156, 119915. <https://doi.org/10.1016/j.ijheatmasstransfer.2020.119915>
- Miller, M. A., Rodrigues, M. A., Glass, M. A., Singh, S. K., Johnston, K. P., & Johnston, K. P. M. (2013). Frozen-state storage stability of a monoclonal antibody: Aggregation is impacted by freezing rate and solute distribution. *International Journal of Pharmaceutical Sciences*, 102(4), 1194–1208. <https://doi.org/10.1002/jps>
- Miyawaki, O., Liu, L., & Nakamura, K. (1998). Effective partition constant of solute between ice and liquid phases in progressive freeze-concentration. *Journal of Food Science*, 63(5), 756–758. <https://doi.org/10.1111/j.1365-2621.1998.tb17893.x>
- Ockman, N. (1958). The infra-red and Raman spectra of ice. *Advances in Physics*, 7(26), 199–220. <https://doi.org/10.1080/00018735800101227>
- Parachalil, D. R., Brankin, B., McIntyre, J., & Byrne, H. J. (2018). Raman spectroscopic analysis of high molecular weight proteins in solution—considerations for sample analysis and data pre-processing. *Analyst*, 143(24), 5987–5998. <https://doi.org/10.1039/c8an01701h>
- Privalov, P. L. (1990). Cold denaturation of protein. *Critical Reviews in Biochemistry and Molecular Biology*, 25(4), 281–306. <https://doi.org/10.3109/10409239009090612>
- Reinsch, H., Spadiut, O., Heidingsfelder, J., & Herwig, C. (2015). Examining the freezing process of an intermediate bulk containing an industrially relevant protein. *Enzyme and Microbial Technology*, 71, 13–19. <https://doi.org/10.1016/j.enzmictec.2015.01.003>
- Rodrigues, M. A., Miller, M. A., Glass, M. A., Singh, S. K., & Johnston, K. P. (2011). Effect of freezing rate and dendritic ice formation on concentration profiles of proteins frozen in cylindrical vessels. *Journal of Pharmaceutical Sciences*, 100(4), 1316–1329. <https://doi.org/10.1002/jps>
- Rodrigues, M. A., Miller, M. A., Glass, M. A., Singh, S. K., & Johnston, K. P. (2012). Comparison of freezing rate and dendritic ice formation on concentration profiles of proteins frozen in cylindrical vessels. *Journal of Pharmaceutical Sciences*, 101(1), 322–332. <https://doi.org/10.1002/jps.22383>
- Roessl, U., Jajcevic, D., Leitgeb, S., Khinast, J. G., & Nidetzky, B. (2014). Characterization of a laboratory-scale container for freezing protein solutions with detailed evaluation of a freezing process simulation. *Journal of Pharmaceutical Sciences*, 103(2), 417–426. <https://doi.org/10.1002/jps.23814>
- Rohleder, D. R., Kocherscheidt, G., Gerber, K., Kiefer, W., Köhler, W., Möcks, J., & Petrich, W. H. (2005). Comparison of mid-infrared and Raman spectroscopy in the quantitative analysis of serum. *Journal of Biomedical Optics*, 10(3), 031108. <https://doi.org/10.1117/1.1911847>

- Savitzky, A., & Golay, M. J. E. (1964). Smoothing and differentiation of data by simplified least squares procedures. *Analytical Chemistry*, 36(8), 1627–1639. <https://doi.org/10.1021/ac60214a047>
- Schmälzlin, E., Moralejo, B., Rutowska, M., Monreal-Ibero, A., Sandin, C., Tarcea, N., Popp, J., & Roth, M. M. (2014). Raman imaging with a fiber-coupled multichannel spectrograph. *Sensors*, 14, 21968–21980. <https://doi.org/10.3390/s141121968>
- Shamlou, P. A., Breen, L. H., Bell, W. V., Pollo, M., & Thomas, B. A. (2007). A new scalable freeze–thaw technology for bulk protein solutions. *Biotechnology and Applied Biochemistry*, 46(1), 13–26. <https://doi.org/10.1042/BA20060075>
- Shevchenko, N., Roshchupkina, O., Sokolova, O., & Eckert, S. (2015). The effect of natural and forced melt convection on dendritic solidification in Ga–In alloys. *Journal of Crystal Growth*, 417, 1–8. <https://doi.org/10.1016/j.jcrysgro.2014.11.043>
- Shukla, A. A., Wolfe, L. S., Mostafa, S. S., & Norman, C. (2017). Evolving trends in mAb production processes. *Bioengineering & Translational Medicine*, 2(1), 58–69. <https://doi.org/10.1002/btm2.10061>
- Singh, S. K., & Nema, S. (2010). Freezing and thawing of protein solutions. In F. Jameel & S. Hershenson (Eds.), *Formulation and process development strategies for manufacturing biopharmaceuticals* (pp. 625–675). John Wiley & Sons, Inc. <https://doi.org/10.1002/9780470595886.ch26>
- Torres, J. F., Komiya, A., Okajima, J., & Shigenao, M. (2012). Measurement of the molecular mass dependence of the mass diffusion coefficient in protein aqueous solutions. *Defect and Diffusion Forum*, 326–328, 452–458. <https://doi.org/10.4028/www.scientific.net/DDF.326-328.452>
- Twomey, A., Kurata, K., Nagare, Y., Takamatsu, H., & Aksan, A. (2015). Microheterogeneity in frozen protein solutions. *International Journal of Pharmaceutics*, 487(1–2), 91–100. <https://doi.org/10.1016/j.ijpharm.2015.04.032>
- Vankeirsbilck, T., Vercauteren, A., Baeyens, W., Van der Weken, G., Verpoort, F., Vergote, G., & Remon, J. P. (2002). Applications of Raman spectroscopy in pharmaceutical analysis. *TrAC Trends in Analytical Chemistry*, 21(12), 869–877. [https://doi.org/10.1016/S0165-9936\(02\)01208-6](https://doi.org/10.1016/S0165-9936(02)01208-6)
- Vynnycky, M., & Kimura, S. (2007). An analytical and numerical study of coupled transient natural convection and solidification in a rectangular enclosure. *International Journal of Heat and Mass Transfer*, 50(25–26), 5204–5214. <https://doi.org/10.1016/j.ijheatmasstransfer.2007.06.036>
- Wang, X., & Fautrelle, Y. (2009). An investigation of the influence of natural convection on tin solidification using a quasi two-dimensional experimental benchmark. *International Journal of Heat and Mass Transfer*, 52(23–24), 5624–5633. <https://doi.org/10.1016/j.ijheatmasstransfer.2009.05.030>
- Weber, D., & Hubbuch, J. (2021). Temperature based process characterization of pharmaceutical freeze-thaw operations. *Frontiers in Bioengineering and Biotechnology*, 9, 617770. <https://doi.org/10.3389/fbioe.2021.617770>
- Weber, D., Sittig, C., & Hubbuch, J. (2021). Impact of freeze-thaw processes on monoclonal antibody platform process development. *Biotechnology and Bioengineering*, 118(10), <https://doi.org/10.1002/bit.27867>
- Wold, S., Sjöström, M., & Eriksson, L. (2001). PLS-regression: A basic tool of chemometrics. *Chemometrics and Intelligent Laboratory Systems*, 58(2), 109–130. [https://doi.org/10.1016/S0169-7439\(01\)00155-1](https://doi.org/10.1016/S0169-7439(01)00155-1)

SUPPORTING INFORMATION

Additional Supporting Information may be found online in the supporting information tab for this article.

How to cite this article: Weber, D., Hubbuch, J. (2021). Raman spectroscopy as a process analytical technology to investigate biopharmaceutical freeze concentration processes. *Biotechnology and Bioengineering*, 1–12. <https://doi.org/10.1002/bit.27936>